Analog Joint Source-Channel Coding with Non-Gaussian Sets of Sensor Samples

Rafaela Schroeder, Glauber Brante, Eduardo Alves Hodgson and Richard Demo Souza

***Abstract*— This work presents an analog joint source-channel coding scheme as an alternative for machine-type communications that require low latency. We have implemented parametric and non-parametric coding for non-Gaussian sets of samples, collected by sensors of temperature and humidity. Since the parametric mappings are optimal only for Gaussian sources, the Box-Cox transformation was used in order to improve performance. Furthermore, we have employed non-parametric coding, which adapts more efficiently to the data sets, further improving performance at the cost of greater complexity.**

***Keywords*— Analog Joint Source-Channel Coding, Non-Gaussian Samples, Machine-Type Communications.**

I. Introduction

In the last few years, the growth of machine-type communications (MTC) rapidly became an enabler for many internet of things applications [1]. For example, MTC applications involve sensors and actuators collecting information continuously to maintain the stability of an industrial plant [2]. In these situations, the delay in communication could result in loss of plant stability, and consequently financial losses. Thus, in many so-called critical-MTC applications, one of the main concerns lies in building ultra-reliable and low latency communication (URLLC) methods.

Traditionally, MTC employs digital communication systems, in which the source of information is primarily encoded with the desired rate/distortion pair. Then, channel codes that operate as close as possible to the Shannon capacity are applied. Such separation between channel and source codes is optimal when large codewords are used [3]. Clearly, the disadvantage is that considerable complexity and delays are introduced due to the block sizes required to approach the theoretical limits. In addition, the digital system is usually designed for one specific rate/distortion pair, so that when the coding rate or target distortion needs to be modified, a complete system remodeling is required to maintain the desired performance.

Alternatively, the analog joint source-channel coding (JSCC) may be inserted in the context of URLLC applications, which require low delay. In such schemes, each symbol of the source is encoded by an analog mapping curve and transmitted through the wireless channel. Thus, source and channel coding are done in only one step, symbol by symbol, resulting in a significant decrease in terms of delay [4]. The use of analog mapping curves was initially proposed concomitantly by Shannon [5] and Kotel'nikov [6], whose idea is to transform N source symbols into K symbols to be transmitted by the channel, resulting in an N:K scheme.

Based on the Shannon-Kotel'nikov mappings, the works in [7]–[9] implemented several schemes either for bandwidth compression ($N > K$) or expansion ($N < K$) in the additive white Gaussian noise (AWGN) channel. In the 2:1 compression scheme, *e.g.*, the achieved performance is very efficient, especially for high channel signal-to-noise channel ratio (CSNR) where the distance from the theoretical limit is of only 1 dB. Moreover, the authors in [10] show that analog JSCC performs very close to the unrestricted capacity of digital schemes, but with considerably smaller complexity than the capacity achieving digital solutions. Furthermore, [11] proposes some strategies to increase the robustness of analog coding in wireless channels, modeled by Rayleigh fading.

Another way to perform the analog mappings is through non-parametric algorithms. Unlike the previously mentioned parametric curves, the non-parametric mapping method employs vector quantizations in the optimization process, aiming to obtain the curve that minimizes the distortion with respect to the information source. In literature, the power constrained channel optimized vector quantization (PCCOVQ) has been proposed in [12] in order to determine optimal mappings for the AWGN channel. Subsequently, the PCCOVQ was further extended to fading channels in [13], [14], yielding efficient performance, approaching the optimal performance theoretically attainable (OPTA).

It is important to notice that the performance of the analog mappings is optimal when the probability density function (PDF) of the source is the same as that of the channel [15]. The optimized mappings from [12] corroborate to this fact when the transmission of Gaussian sources over an AWGN channel is considered, by exhibiting mappings that resemble the parametric curves used in [7]–[9], which are optimized for the same scenario. However, many MTC applications do not necessarily involve Gaussian signals. For example, usual measurements taken by sensors, such as temperature and humidity, can hardly be used directly with the above-mentioned mappings. This motivates the investigation of techniques to ensure good performance of analog schemes with non-Gaussian sources.

In this work, we adopted two sets of temperature and humidity samples collected by sensors available in [16], which have non-Gaussian PDFs. Therefore, we first implement sim-

Rafaela Schroeder and Glauber Brante, Federal University of Technolgy - Paraná (UTFPR), Curitiba, Brazil. E-mails: rschroeder@alunos.utfpr.edu.br, gbrante@utfpr.edu.br. Eduardo A. Hodgson, UTFPR, Cornélio Procópio. E-mail: hodgson@utfpr.edu.br. Richard D. Souza, Federal Universitu of Santa Catarina (UFSC), Florianópolis. E-mail: richard.demo@ufsc.br. This study was financed in part by the Coordenação de Aperfeiçoamento de Pessoal de Nível Superior - Brasil (CAPES) - Finance Code 001, and CNPq.

ple techniques to improve the performance of the parametric schemes. To that end, we have employed the Box-Cox transformation, which performs power functions in order to approach the arbitrary PDF of the collected data to that of a Gaussian source [17]. The advantage of combining the parametric mappings with the Box-Cox transformation is the low complexity, which may be crucial to practical MTC implementations. On the other hand, since the non-parametric schemes adapt more efficiently to different data sets, we have also employ the PCCOVQ algorithm following [14]. Our results show that the non-parametric scheme has increased performance, at the cost of a greater complexity due to the optimizations required by the PCCOVQ algorithm. However, for some CSNR values we observe that both mappings perform similarly, with less than 1 dB of difference between them. Thus, the parametric mapping also stands out as a good alternative with lower implementation complexity. With respect to the OPTA, there a difference of 6 dB at the CSNR of 15 dB using the parametric scheme for the temperature set, while the non-parametric scheme reduces this difference to 5.2 dB.

The remainder of this paper is organized as follows. Section II describes the system model, the proposed combination of parametric mappings and the Box-Cox transformation is given by Section III, while the PCCOVQ algorithm is given by Section IV. Section V presents some numerical results and, finally, Section VI concludes the paper.

II. System Model

Analog JSCC is based on coding discrete-time continuous amplitude symbols using a mapping curve. Let us consider a source vector $\mathbf{x} \in \mathbb{R}^{1\times N}$, with mean power $\sigma_{\mathbf{x}}^2$, which is encoded into $\mathcal{C}(\mathbf{x}) \in \mathbb{R}^{1\times K}$ using either parametric or non-parametric mappings. The resulting coded vector is then transmitted through the wireless channel. At the receiver, the received signal is given by

$$\mathbf{y} = \mathcal{C}(\mathbf{x}) \cdot h + \mathbf{w}, \tag{1}$$

where h is the channel fading coefficient, modeled according to a quasi-static Rayleigh distribution with power σ_h^2, while $\mathbf{w}$ is the AWGN vector, with variance $\sigma_{\mathbf{w}}^2$. Then, the CSNR is defined as

$$\text{CSNR} = 10\log_{10}\left(\frac{\sigma_h^2}{\sigma_{\mathbf{w}}^2}\right). \tag{2}$$

To evaluate the performance, a frequently used metric is the mean squared error (MSE), which computes the Euclidean distance between $\mathbf{x}$ and the estimate $\hat{\mathbf{x}}$ obtained by the receiver based on $\mathbf{y}$,

$$\text{MSE} = \frac{\|\mathbf{x}-\hat{\mathbf{x}}\|^2}{N}, \tag{3}$$

from which we write the signal-to-distortion ratio (SDR) as

$$\text{SDR} = 10\log_{10}\left(\frac{\sigma_{\mathbf{x}}^2}{\text{MSE}}\right). \tag{4}$$

Furthermore, the theoretical limit of communication is given by the OPTA, obtained by equating the channel capacity and the rate distortion function, so that [11]

$$N\log_{10}\left(\frac{\sigma_{\mathbf{x}}^2}{\text{MSE}}\right) = K\int_h 10\log_{10}\left(1+\frac{h^2}{\sigma_{\mathbf{w}}^2}\right)p(h)\,\mathrm{d}h. \tag{5}$$

Throughout this work, we focus on 2:1 compression schemes, *i.e.*, $N = 2$ source symbols are encoded into $K = 1$ channel symbol. In the sequel, Section III details parametric mappings, while the PCCOVQ algorithm is given in Section IV.

III. Parametric Scheme

A. Box-Cox Transformation

In order to improve performance of non-Gaussian sources using parametric analog mappings, we first resort to the Box-Cox transformation, which aims to approach the PDF of the collected data to a Gaussian PDF [17]. Then, for a source symbol vector $\mathbf{s}$ with arbitrary distribution, the Box-Cox transformation is given by

$$\mathbf{s}(\mu) = \begin{cases} \ln(\mathbf{s}), & \mu = 0 \\ \dfrac{\mathbf{s}^\mu - 1}{\mu}, & \mu \neq 0 \end{cases} \tag{6}$$

in which $-5 \leq \mu \leq 5$ is numerically optimized in order to obtain a PDF as close as possible to a Gaussian distribution.

Moreover, in order to obtain a set of samples with zero-mean, we normalize the data using

$$\widetilde{\mathbf{s}} = \frac{\mathbf{s}(\mu) - \overline{\mathbf{s}}(\mu)}{\max\{\mathbf{s}(\mu)\} - \min\{\mathbf{s}(\mu)\}}, \tag{7}$$

where $\overline{\mathbf{s}}(\mu)$ denotes the mean of the vector $\mathbf{s}(\mu)$.

B. 2:1 Compression

One of the most employed parametric mappings in the case of 2:1 compression is known as the Archimedes' spiral curve, which encodes a pair of samples $\mathbf{x} = (x_1, x_2) \subset \widetilde{\mathbf{s}}$ on the positive and negative arms of the spiral, whose corresponding angles are given by [7]

$$\hat{\theta}_1 = \arg\min_{\theta\geq 0}\{(x_1 - \frac{\Delta}{\pi}\theta\sin\theta)^2 + (x_2 - \frac{\Delta}{\pi}\theta\cos\theta)^2\}, \tag{8}$$

$$\hat{\theta}_2 = \arg\min_{\theta< 0}\{(x_1 + \frac{\Delta}{\pi}\theta\sin\theta)^2 + (x_2 - \frac{\Delta}{\pi}\theta\cos\theta)^2\}, \tag{9}$$

where Δ is the distance between the arms of the spiral, and $\theta \in \mathbb{R}$ is the angle that corresponds to the path between the origin to the point mapped in the spiral. Finally, we employ only the smaller angle, so that the mapping is defined as

$$M_\Delta(\mathbf{x}) = \min(\hat{\theta}_1, \hat{\theta}_2). \tag{10}$$

Figure 1 illustrates the encoding of a pair of samples on the Archimedes' spiral curve. As an example, we adopted $\mathbf{x} = (1.3, 1.3)$, represented by the symbol $\circ$ in the figure. Then, positive and negative angles θ_1 and θ_2 are shown, so that $M_\Delta(\mathbf{x}) = \theta_2$ is chosen as the mapped symbol, represented by $*$ in the figure. As a result, two source symbols represented by coordinates of the Cartesian plane are mapped into a single angle $M_\Delta(\mathbf{x})$ on Archimedes' spiral.

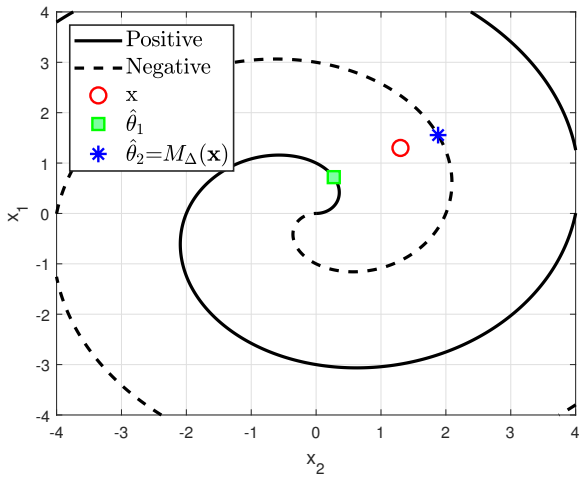

Fig. 1: Example of a pair of samples $\mathbf{x} = (1.3, 1.3)$ mapped into the Archimedes' spiral, resulting in a single symbol $M_\Delta(\mathbf{x})$.

In addition, following [9], [11], we also employ an invertible function T_α, so that

$$T_\alpha\left(M_\Delta(\mathbf{x})\right) = \text{sign}(M_\Delta(\mathbf{x})) \cdot |M_\Delta(\mathbf{x})|^\alpha, \qquad (11)$$

where α becomes a parameter to be optimized together with Δ, which allows to increase the SDR at the receiver [11].

Finally, we normalize the energy of the channel symbol using a parameter γ, so that the symbol to be transmitted through the wireless channel is given by

$$\mathcal{C}(\mathbf{x}) = \frac{T_\alpha\left(M_\Delta(\mathbf{x})\right)}{\gamma}. \qquad (12)$$

C. Decoding

At the receiver, the received symbol denoted by y is denormalized by γ, has its phase adjusted and receives the inverse function $T_\alpha^{-1}(\cdot)$, so that

$$\widetilde{y} = \text{sign}\left(\frac{y \cdot \gamma}{h}\right) \cdot \left|\frac{y \cdot \gamma}{h}\right|^{\frac{1}{\alpha}}. \qquad (13)$$

Then, an estimate $\hat{\mathbf{x}}$ is made based on $\widetilde{y}$ using a maximum likelihood (ML) decoder, given by [9]

$$\hat{\mathbf{x}}_{\text{ML}} = M_\Delta^{-1}\left(\widetilde{y}\right), \qquad (14)$$

where $M_\Delta^{-1}(\cdot)$ is the inverse mapping.

Finally, the inverse of the Box-Cox transformation involves operations of (6)-(7), such that

$$\widetilde{\mathbf{s}}_{\text{ML}} = \hat{\mathbf{x}}_{\text{ML}} \cdot \Big(\max\{\mathbf{s}(\mu)\} - \min\{\mathbf{s}(\mu)\}\Big) + \overline{\mathbf{s}}(\mu), \qquad (15)$$

in which it is assumed that $\min\{\mathbf{s}(\mu)\}$, $\max\{\mathbf{s}(\mu)\}$ and $\overline{\mathbf{s}}(\mu)$ are known at the receiver. Then, by applying μ, also known, we have the estimation of the transmitted signal given by

$$\hat{\mathbf{s}} = \left(\widetilde{\mathbf{s}}_{\text{ML}} \cdot \mu + 1\right)^{\frac{1}{\mu}}. \qquad (16)$$

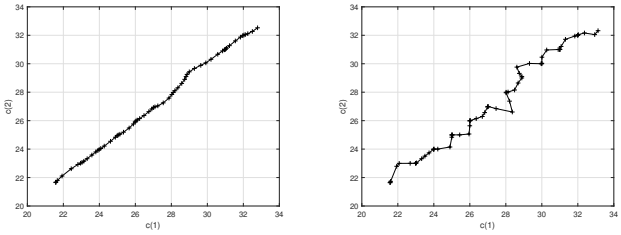

(a) $h = 1.4$, (b) $h = 3.0$.

Fig. 2: Mappings obtained with the PCCOVQ algorithm for the employed set of temperatures.

IV. Non-Parametric Scheme

Non-parametric encoding determines the optimal mapping for a given data-set by performing numerical optimizations. In this work, we have employed the PCCOVQ algorithm, following [13], [14], which aims at mapping the vector $\mathbf{x}$ of $N = 2$ dimensions in Q quantization regions Ω_i, obtaining a partition $\mathbf{p} = \{\Omega_0, \Omega_1, \cdots, \Omega_{Q-1}\}$. Then, the encoder selects a channel symbol given by $s = \Delta_{\text{P}} \cdot u_i$, where u_i is a signal from a pulse amplitude modulation (PAM) and Δ_{p} is the constant distance between two neighboring symbols. In addition, the receiver is composed by a set of a codebooks $\mathbf{a}$, which contain the reconstruction vectors $\mathbf{c}_{k,j}$ that allow decoding. Therefore, the parameters $\mathbf{p}$, $\mathbf{a}$ and Δ_{P} are optimized according to

$$\min_{\mathbf{p},\mathbf{a},\Delta_{\text{P}}} D(\mathbf{p}, \mathbf{a}, \Delta_{\text{P}}) + \lambda P, \qquad (17)$$

whose goal is to minimize the distortion between the original and the mapped symbols, $D(\mathbf{p}, \mathbf{a}, \Delta_{\text{P}})$, according to the MSE criterion in (3), with λ being a Lagrange multiplier to constrain the employed power P.

For the sake of brevity, we briefly present the optimization process in (17), done by the Linde-Buzo-Gray (LBG) algorithm [18]. In addition, we also refer to [14] for a more detailed description of the algorithm. Then, the LBG algorithm involves five steps:

1. Initialization of the algorithm with fixed values of Δ_{p}, λ and a known codebook;
2. Optimization of the partition $\mathbf{p}$;
3. Optimization of the coodebook $\mathbf{a}$;
4. Optimization of the parameter Δ_{p};
5. Calculation of $D(\mathbf{p}, \mathbf{a}, \Delta_{\text{P}})$ and, if the decrease in terms of MSE between two consecutive iterations is smaller than a predefined threshold, the optimization is stopped; otherwise, repeat from step 2.

Figure 2 illustrates the mappings obtained by the PCCOVQ algorithm to the set of temperatures from [16], for different fading values. Nevertheless, since the instantaneous fading coefficient is not known by the receiver, a distortion is still expected afer decoding.

V. Numerical Results

In this work, we have used temperature and humidity samples available in [16], collected in Athens, Greece, in 2018. The temperature set has 1310 samples ranging from

TABELA I: Information about the dataset.

General Information	Temperature (°C)	Humidity (%)
Number of samples	1310	812
Minimum value	20	25
Maximum value	42	45
Mean	32.70	38.33
Variance	27.94	11.09

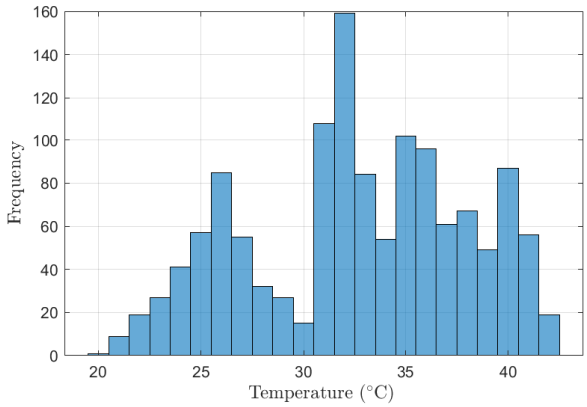

(a) Temperature set.

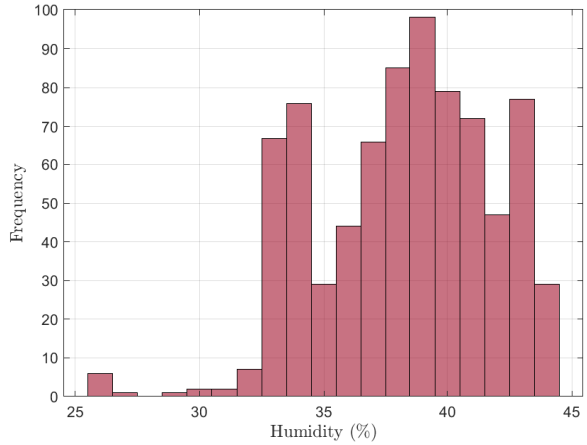

(b) Relative humidity set.

Fig. 3: Histograms of the employed data-sets [16].

20°C to 42°C, while the relative humidity set has 812 samples ranging from 25% to 45%. Table I summarizes the information of the collected data and Figure 3 illustrates the histograms of each data-set, from which we can observe non-Gaussian distributions.

First, in order to evaluate the application of the Box-Cox transformation for each data-set we employ the Kolmogorov-Smirnov (KS) test [19], which evaluates the normality of a given sample distribution by means of a probability of significance P_{S}. Then, to affirm that a given set of samples is Gaussian distributed, it is necessary that P_{S} falls above a certain level of significance threshold, usually adopted as $P_{\mathrm{S}} > 0.05$. Table II shows the values of P_{S} for the original sets of temperature and humidity, as well as the sets after the Box-Cox transformation. As we can observe, the KS test shows that the Box-Cox transformation does not provide

TABELA II: Probability of significance (P_{S}), before and after Box-Cox transformation.

Set	Original Samples	Transformed Samples
Temperature	$8.5296 \cdot 10^{-7}$	$2.5334 \cdot 10^{-5}$
Humidity	$1.7067 \cdot 10^{-4}$	0.0014

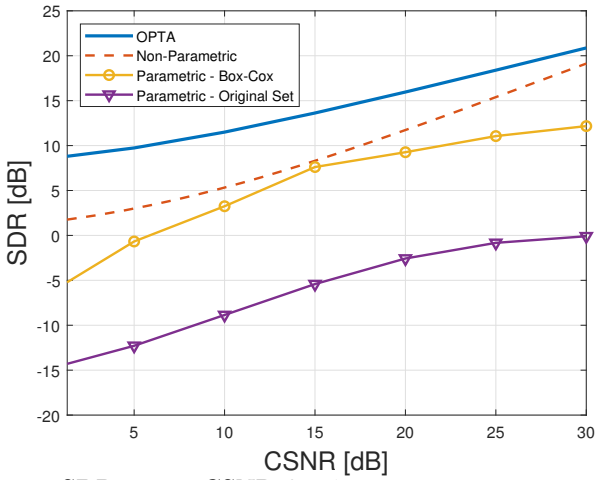

Fig. 4: SDR versus CSNR for the temperature set.

perfect Gaussian distributions, according to the established level of significance. Given that there are significant gaps in the histograms presented by Figure 3, which are inherent characteristics of the adopted sample sets, the normalization of the data becomes limited. However, let us remark that the value of P_{S} after the Box-Cox transformation is significantly larger than for the original sets. As we will observe in the following results, such an increment is already important to improve the performance.

Figure 4 shows the SDR performance as a function of the CSNR for the set of temperature samples. We consider the parametric scheme with and without the Box-Cox transformation, denoted respectively by 'Box-Cox' and 'Original', the non-parametric scheme by means of the PCCOVQ algorithm, and the OPTA. As we can observe, the non-parametric scheme achieves better performance, with a difference of approximately 7 dB with respect to the OPTA in low CSNR, reducing while the CSNR increases. For the parametric scheme, it is first important to notice the significant SDR improvement yielded by the Box-Cox transformation, confirming the effectiveness of the method. In addition, we can also observed that its performance is very close to the non-parametric scheme for a CSNR around 15 dB, thus becoming a good low-complex alternative method. However, we also observe that the SDR of this method stagnates at high CSNR, which is due to the mismatch between the PDF of the samples and that of the channel. Despite the improvements provided by the Box-Cox transformation, the KS test shows that there is still a considerable difference between the transformed data-set and the Gaussian PDF, which is evidenced in higher CSNRs.

In addition, we numerically optimize the parameters α and Δ in order to maximize the SDR of the parametric mappings, for each data-set. The optimized values are given in Tables III

TABELA III: Optimization of the parameter α.

CSNR [dB]	0	5	10	15	20	25	30
Temp. Original	20.3	16.9	16.3	16.0	16.9	19.7	18.0
Temp. Box-Cox	1.0	1.5	1.5	1.5	2.0	2.0	2.0
Humidity Original	15	19.7	18.7	19.9	20.6	22.2	23.8
Humidity Box-Cox	1.0	1.5	1.5	1.5	2.0	2.0	2.0

TABELA IV: Optimization of the parameter Δ.

CSNR [dB]	0	5	10	15	20	25	30
Temp. Original	34	34	34	36	37	37	37
Temp. Box-Cox	3.9	3.25	3.0	2.0	2.0	2.0	2.0
Humidity Original	37	37	40	42	43	43	43
Humidity Box-Cox	3.9	3.25	3.0	2.0	2.0	2.0	2.0

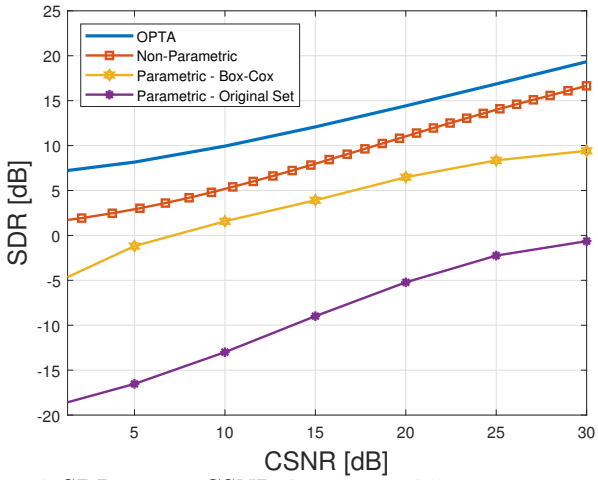

Fig. 5: SDR versus CSNR for the humidity set.

and IV, respectively. As observed in our simulations, the optimization of α and Δ without the application of the Box-Cox transformation performs quite far from theoretical limit, 18 dB from the OPTA at CSNR $=$ 20 dB for the set of temperatures, while the Box-Cox transformation is able to reduce this gap to 7 dB. Therefore, the difference caused by the Box-Cox transformation is more expressive than the optimization of α and Δ alone.

Finally, Figure 5 plots the SDR as a function of the CSNR for the set of humidity samples, for which we can draw very similar conclusions, demonstrating the adaptability of the methods. A noteworthy comparison between Figures 4 and 5 is the absolute values of the SDR. Since the SDR depends on the variance of the source, so that $\sigma_{\mathbf{x}}^2 = 27.94$ for the adopted set of temperatures and $\sigma_{\mathbf{x}}^2 = 11.09$ for the set of humidity, there is a small difference in terms of SDR comparing the two figures. Therefore, the obtained conclusions are always drawn with respect to the corresponding OPTA.

VI. Conclusion

In light of the growing demand for MTC applications requiring low latency, we have evaluated the performance of analog JCSS schemes considering sets of temperature and humidity samples collected by sensors, which have non-Gaussian distributions, common to MTC scenarios. Then, two distinct analog coding methods have been considered, denoted by parametric and non-parametric schemes. The former has low implementation complexity, but it has low performance when operating with non-Gaussian sources. Therefore, we have proposed the use of the Box-Cox transformation in order to improve performance. The latte scheme was implemented based on the PCCOVQ algorithm, which yields optimized mappings, resulting in a performance quite close to the theoretical limit, at the cost of a higher implementation complexity. Our results have shown that the Box-Cox transformation is able to considerably increase the performance of the parametric method, being at a distance of 6 dB from the OPTA when CSNR $=$ 15 dB. Furthermore, the non-parametric scheme is able to improve performance even further, reducing this gap ith respect to the OPTA to 5.2 dB.

References

[1] J. Yuan, H. Shan, A. Huang, T. Q. Quek, and Y.-D. Yao, "Massive machine-to-machine communications in cellular network: Distributed queueing random access meets MIMO," *IEEE Access*, vol. 5, pp. 2981–2993, 2017.

[2] P. Nouri, H. Alves, R. D. Souza, and M. Latva-aho, "Ultra-reliable short message cooperative relaying protocols under Nakagami-m fading," in *Int. Symp. on Wireless Commun. Systems (ISWCS)*, 2017, pp. 287–292.

[3] C. E. Shannon, "A mathematical theory of communication," *Bell Syst. Tech. J.*, vol. 27, pp. 379–423; 623–656, 1948.

[4] T. A. Ramstad, "Shannon mappings for robust communication," *Telektronikk*, vol. 98, no. 1, pp. 114–128, 2002.

[5] C. E. Shannon, "Communication in presence of noise," in *Proc. IRE*, vol. 37, 1949, pp. 10–21.

[6] V. A. Kotel'nikov, *The theory of optimum noise immunity*. McGraw-Hill, 1959.

[7] F. Hekland, P. A. Floor, and T. A. Ramstad, "Shannon-Kotelnikov mappings in joint source-channel coding," *IEEE Trans. Commun.*, vol. 57, no. 1, pp. 94–105, 2009.

[8] P. Suárez-Casal, Ó. Fresnedo, L. Castedo, and J. García-Frías, "Parametric analog mappings for correlated Gaussian sources over AWGN channels," in *IEEE International Conference on Acoustics, Speech and Signal Processing (ICASSP)*, 2016, pp. 3761–3765.

[9] Y. Hu, J. Garcia-Frias, and M. Lamarca, "Analog joint source-channel coding using non-linear curves and MMSE decoding," *IEEE Trans. Commun.*, vol. 59, no. 11, pp. 3016–3026, Nov. 2011.

[10] O. Fresnedo, F. J. Vazquez-Araujo, J. Garcia-Frias, M. Gonzalez-Lopez, and L. Castedo, "Comparison between analog joint source-channel coded and digital BICM systems," in *IEEE International Conference on Communications (ICC)*, 2011, pp. 1–5.

[11] G. Brante, R. D. Souza, and J. Garcia-Frias, "Spatial diversity using analog joint source channel coding in wireless channels," *IEEE Trans. Commun.*, vol. 61, no. 1, pp. 301–311, Jan. 2013.

[12] A. Fuldseth, "Robust subband video compression for noisy channels with multilevel signaling," *NTNU*, 1997.

[13] A. A. Saleh, F. Alajaji, and W.-Y. Chan, "Power-constrained bandwidth-reduction source-channel mappings for fading channels," in *26th Biennal Symposium on Communications (QBSC)*, 2012, pp. 85–90.

[14] E. A. Hodgson, G. Brante, R. D. Souza, J. García-Frías, and J. L. Rebelatto, "Compensating spectral efficiency loss of wireless RF energy transfer with analog joint source channel coding compression," *IEEE Sensors Journal*, vol. 16, no. 16, pp. 6458–6469, 2016.

[15] T. Goblick, "A coding theorem for time-discrete analog data sources," *IEEE Trans. Inf. Theory*, vol. 15, no. 3, pp. 401–407, 1969.

[16] UCI Machine Learning Repository. (2018, March) GNFUV unmanned surface vehicles sensor data data set. [Online]. Available: https://archive.ics.uci.edu/ml/datasets/GNFUV+Unmanned+Surface+Vehicles+Sensor+Data#

[17] J. W. Osborne, "Improving your data transformations: Applying the box-cox transformation," *Practical Assessment, Research & Evaluation*, vol. 15, no. 12, pp. 1–9, 2010.

[18] K. Sayood, *Introduction to Data Compression*, 3rd ed. Morgan Kaufmann, 2006.

[19] F. J. Massey Jr., "The Kolmogorov-Smirnov test for goodness of fit," *Journal of the American Statistical Association*, vol. 46, no. 253, pp. 68–78, 1951.